Journal of Materials Chemistry A

Accepted Manuscript

ROYAL SOCIETY OF CHEMISTRY

www.rsc.org/materialsA

Manuscript for J. Mater. Chem. A

The influence of alkyl side chains on molecular packing and solar cell performance of dithienopyrrole-based oligothiophenes

Gisela L. Schulz,[a,d] Prasenjit Kar,[a,e] Martin Weidelener,[a] Astrid Vogt,[a] Marta Urdanpilleta,[b] Mika Lindén,[c] Elena Mena-Osteritz,[a] Amaresh Mishra[a,f]* and Peter Bäuerle[a]*

[a]*Institute of Organic Chemistry II and Advanced Materials, Ulm University, Albert-Einstein-Allee 11, 89081 Ulm, Germany*

[b]*Department of Applied Physics I, University of the Basque Country (UPV/EHU), Plaza de Europa, 1, 20018 Donostia, San Sebastián, Spain*

[c]*Institute of Inorganic Chemistry II, Ulm University, Albert-Einstein-Allee 11, 89081 Ulm, Germany*

[d]*Current address: Institute of Polymer Chemistry, University of Stuttgart, Pfaffenwaldring 55, 70569 Stuttgart, Germany*
[e]*Current address: Department of Chemistry, Indian Institute of Technology, Roorkee-247667, India*

[f]*Current address: School of Chemistry, Sambalpur University, Jyoti Vihar-768019, Sambalpur, India*

*E-mail: amaresh.mishra@suniv.ac.in; peter.baeuerle@uni-ulm.de

Keywords: dithienopyrrole, solution-processing, bulk-heterojunction solar cell, metal oxide, solvent additive, morphology

Abstract

The synthesis of a series of dithieno[3,2-*b*:2',3'-*d*]pyrrole (DTP) containing A-D-A oligomers for use in solution-processed bulk heterojunction solar cells is presented. This series allows investigation of the effect of alkyl chains attached to the thiophene moieties or the nitrogen of the DTP unit on the thermal and physical properties of the oligomers. The photoactive layers were probed using absorption spectroscopy, grazing incident X-ray diffraction, and atomic force microscopy. From these experiments, it was found that the hexyl chains attached to the thiophene units are instrumental to obtain good packing and high fill factors in the solar cell devices. For the fabrication of solar cells, both, PEDOT:PSS and V_2O_5, were investigated as hole transport layers and PDMS was employed as solvent additive. High open-circuit voltages of up to 1.1 V, moderate short-circuit current densities, and high fill factors of up to 0.63 were obtained yielding power conversion efficiencies as high as 5.3%.

Introduction

The field of bulk-heterojunction organic solar cells (BHJSC) made of solution-processed (co)oligomers, often referred to as "small molecules", is progressing rapidly. Recently, using functional molecular donors and fullerene-based acceptors power conversion efficiencies (PCE) exceeding 9% have been reported for single junction and 10.1% for homo-tandem solution-processed OSCs.[1-11] An important part of this progress is the judicious design and synthesis of new photoactive materials and optimization of active-layer processing method and several reviews highlighting the structural development over the last years appeared.[12-16] Various design strategies and building blocks have been employed for the preparation of novel molecular materials in order to tune their absorption, packing, and electronic energy levels. An important part of this molecular design is the length and position of solubilizing alkyl chains, which can strongly affect the self-assembly and ordering of the molecules in the bulk. To date, molecules with alkyl chains at the α-positions of terminal thiophene units,[9,17-19] as well as in the β-positions were well investigated.[5,11,19-21] Fur-

thermore, optoelectronic properties were tuned by varying the electron-donating or accepting strength of the building blocks present in the photoactive molecule to modify both, the magnitude and position of the absorption profile as well as the molecular orbital energy levels.[10,22-24] Combining strong donors with strong acceptors in the conjugated chain results in a red-shift of the main absorption band and an increase of the molar extinction coefficient.

Recently, we have reported a series of dithieno[3,2-*b*:2',3'-*d*]pyrrole (DTP)-containing acceptor-donor-acceptor (A-D-A)-type oligomers showing excellent fill factors of up to 0.72 and high PCEs up to 6.1% in solution-processed BHJSCs upon solvent vapor annealing treatment of the active layer.[11] The DTP[25] unit has only rarely been used in the development of oligomeric semiconductors for solar cell applications reaching PCEs in the range of 0.2 to 2.7%.[26-29]

Equally important to having well-designed photoactive materials, is the selection and optimization of an appropriate device structure. Each component must meet specific requirements in order to produce an efficient solar cell. In this respect, the use of metal oxides as charge transport layers has been extensively investigated and described in literature.[30,31] Vanadium, molybdenum, tungsten, and nickel oxides (V_2O_5,[32-35] MoO_3,[32,36,37] WO_3,[38,39] NiO[40-42]) are typically used as hole transport layers, whereas zinc oxide (ZnO)[43-46] and titanium dioxide (TiO_2)[47,48] have been employed as electron transport layers.[49,50] Metal oxides are good candidates for charge transport materials due to their high optical transparency, tunable work functions, and semiconducting properties. Improvements in solar cell performance have been attributed to increased charge collection, hole or electron blocking properties, reduced charge recombination, and/or optical spacer effects. In a recent report, Heeger *et al.* have demonstrated an improvement of PCE from 6.0% to 8.9% by incorporation of ZnO as electron extraction layer.[1] Another important aspect is the use of metal oxides for Ohmic contacts to maximize the V_{OC} because the reduction of built-in potential leads to an increase in dark current as well as carrier recombination.[31]

In this work, a series of A-D-A oligomers consisting of terminal dicyanovinylene (DCV) groups and a central DTP unit linked by thiophene or hexyl-substituted thiophene units were designed and

synthesized. The DCV groups are known to provide balanced acceptor strength and strong intermolecular interactions in the solid state.[51] The combination with an electron-rich DTP moiety results in materials with red-shifted absorption and very high molar extinction coefficients. Such type of oligomers were incorporated into solution-processed BHJSC as electron donor materials and fullerene [6,6]-phenyl-C_{61}-butyric acid methyl ester ($PC_{61}BM$) as electron acceptor. Device architectures containing either PEDOT:PSS or V_2O_5 as hole transport layer (HTL) were investigated. The best devices using V_2O_5 as HTL and polydimethylsiloxane (PDMS) as solvent additive resulted in PCEs up to 5.3%. Thin-film absorption, atomic force microscopy, and grazing incident X-ray diffraction measurements were perform to further understand the morphology of the photoactive layer.

Results and discussion

The four DTP-containing oligomers were synthesized by Pd^0-catalyzed Stille-type coupling as shown in Scheme 1. The synthesis of DCV-substituted bromothiophene **6** is reported elsewhere.[52] DCV-substituted iodothiophene **7** was prepared in high yield and is shown in detail in Scheme S1 (see ESI†). The Stille-coupling reaction of either **6** or **7** with bisstannylated DTP **5a**,**b** gave the target compounds in yields between 73-83%. The obtained oligomers **1**-**4** were purified using high performance liquid chromatography (HPLC) before they were further characterized.

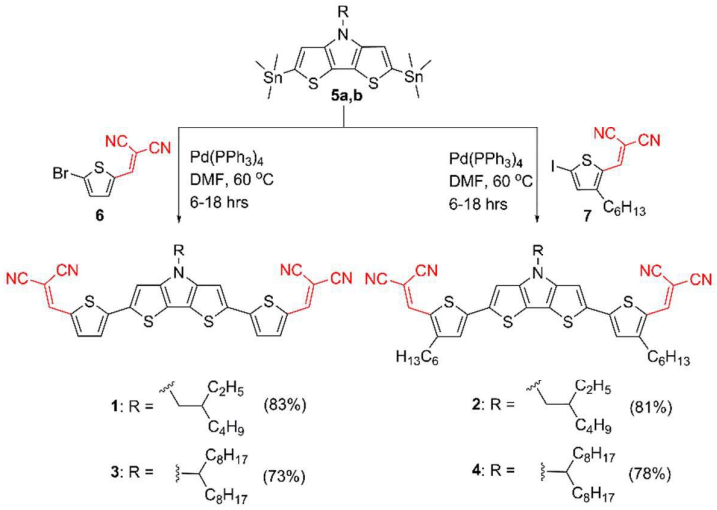

Scheme 1. Synthesis of dithieno[3,2-*b*:2',3'-*d*]pyrrole-based A-D-A oligomers **1**-**4**.

The melting points of all oligomers **1**-**4** were determined by differential scanning calorimetry (DSC). In the DSC curves, they displayed one sharp endothermic peak whereby T_m indicates the melting temperature. The replacement of the branched ethylhexyl substituent attached to the central nitrogen in **1** and **2** by a larger octylnonyl in **3** and **4** lowered T_m. All oligomers were found to be stable up to 330 °C and only showed decomposition on further heating which is indicated by a broad exothermic peak in the DSC curves (Figure 1).

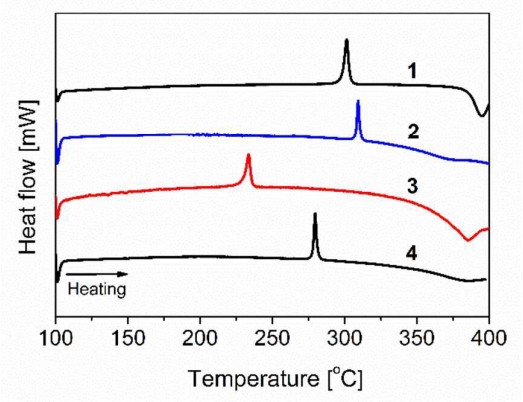

Figure 1. DSC trace of all A-D-A oligomers **1**-**4** measured under Ar flow at heating rate of 10 °C/min.

UV-vis absorption spectroscopy was performed on solutions and thin films spin-coated from chloroform (Figure 2 and Table 1). High molar extinction coefficients of ~100 000 M^{-1} cm^{-1} with absorption maxima at approximately 600 nm were observed for oligomers **1** to **4** due to the strong D-A charge transfer character of the DTP donor and the DCV acceptor. Absorption spectra of thin films revealed a red-shifted main absorption band compared to the measurements performed in solution with maxima at 680 nm. The film spectra displayed a shoulder at higher energy at around 610 nm for this band. The structured absorption and sharp onset at longer wavelength is indicative of good ordering of the molecules which will be discussed later.

The maximum solubility of the oligomers in chloroform was determined to assess their potential for solution-processed solar cells (Table 1). The solubility of oligomer **1** (0.2 mg mL^{-1}) unfortunately was insufficient for thin film preparation by spin-coating. The solubility of **2** was increased to 2

mg mL^{-1} as a result of the additional hexyl chains on the thiophene backbone. Oligomers **3** and **4** displayed even further enhancement of the solubility to 19 and 27 mg mL^{-1}, respectively, upon exchange of the ethylhexyl by the larger octylnonyl substituent.

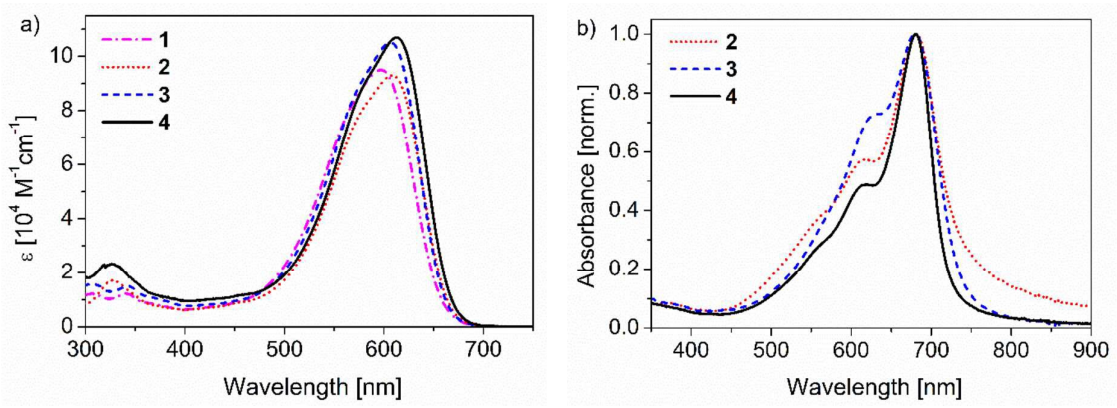

Figure 2. a) UV-Vis spectra of oligomers **1-4** measured in chloroform solution. b) Normalized absorption spectra of the oligomers in thin films prepared by spin-coating onto glass substrates (4 mg/mL in chloroform).

Table 1. UV-Vis absorption and electrochemical, melting temperature and maximum solubility data of oligomers **1-4**.

Oligomer	λ_{abs} sol [nm][a]	ε [M^{-1} cm^{-1}]	ΔE_{opt} sol [eV]	λ_{abs} film [nm][b]	ΔE_{opt} film [eV]	E^0_{ox1} [V][c]	E^0_{ox2} [V][c]	$E_{p\,red}$ [V][c]	HOMO [eV][d]	LUMO [eV][d]	ΔE_{CV} [eV]	T_m [°C][e]	Solubility [mg/mL][f]
1	597	95 000	1.89	-	-	0.51	1.09	-1.36	-5.54	-3.84	1.70	301	0.2
2	609	92 200	1.88	681	1.82	0.45	1.03	-1.43	-5.49	-3.68	1.81	309	2
3	605	105 000	1.87	680	1.83	0.55	1.14	-1.44	-5.58	-3.81	1.77	233	19
4	612	107 000	1.87	680	1.83	0.53	1.10	-1.53	-5.55	-3.78	1.77	280	27

[a]Absorption spectra were measured in chloroform. [b]Thin films were spin-coated from chloroform solutions (4 mg/mL) on glass substrate at 3000 rpm. [c]Cyclic voltammetry was performed in dichloromethane/$TBAPF_6$ (0.1 M), scan rate = 100 mV/s, referenced against Fc/Fc$^+$. The oxidation potentials ($E°_{ox}$) were calculated by means of cathodic and anodic peak potentials of quasi-reversible waves: $E° = (E_{pa}+E_{pc})/2$. For the irreversible waves, E_p values are given. [d]HOMO/LUMO energy values were calculated by setting Fc/Fc$^+_{vac}$ at -5.1 eV vs vacuum. [e]Melting temperatures (T_m) were determined using differential scanning calorimetry. [f]Solubility was measured in chloroform.

Electrochemical measurements were performed on the series of oligomers **1-4** in solution in order to determine the energy levels the frontier orbitals. The data is shown in Figure 3 and summarized in Table 1. The redox properties are nearly similar for all four compounds. Two reversible oxidation waves at around 0.5V and 1.1 V are observed due to formation of stable radical cations and dications on the oligomeric backbone. When scanning to negative potentials, an irreversible reduction at ~ -1.4 V, which is typical for DCV acceptor groups, was seen. From the onset of the first oxidation and reduction potential, HOMO and LUMO energies were calculated and lie around -5.5 eV (HOMO) and -3.7 to -3.8 eV, respectively. These values should be well compatible with the

energy levels of $PC_{61}BM$ (HOMO = -6.1 eV, LUMO = -4.0 eV[53]) to ensure efficient electron transfer from the donor to the acceptor.

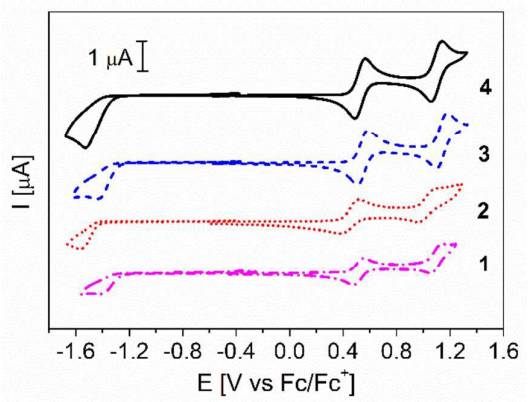

Figure 3. Cyclic voltammograms of oligomers **1-4** in (1×10^{-3} mol L^{-1} in dichloromethane/*n*-Bu_4NPF_6 as supporting electrolyte). All scan rates were 100 mV s^{-1} and the potentials were internally referenced to the Fc/Fc^+ couple.

In order to obtain insight into the molecular packing behavior of oligomers **2-4** in the solid state, grazing incident X-ray diffraction (GIXRD) experiments were performed on neat films. The resulting diffraction patterns are plotted in Figure 4. All oligomers displayed a relatively intense (100) reflection peak at low angle (2θ = 5.95° for **2**, 6.18° for **3**, 5.13° for **4**) indicating the presence of crystalline domains. This low angle reflection is assigned to the d_{100} spacing and correlates to the separation between the oligothiophene backbones and is directly related to the type and the presence or absence of the alkyl substituents. Oligomers **2** and **3** containing an ethylhexyl chain attached to the DTP-nitrogen showed a d_{100}-spacing of 14.8 Å and 14.3 Å, respectively, whereas oligomer **4** comprising the larger octylnonyl chain gave an increased d_{100} spacing of 17.2 Å. The broad reflex seen between 2θ = 7−15° originates from a combination of donor, acceptor, and the substrate. The XRD-measurements on the neat films provide qualitative information regarding the packing behavior of the molecules and as well facilitate peak assignment in the diffraction pattern obtained for the blend films (*vide infra*).

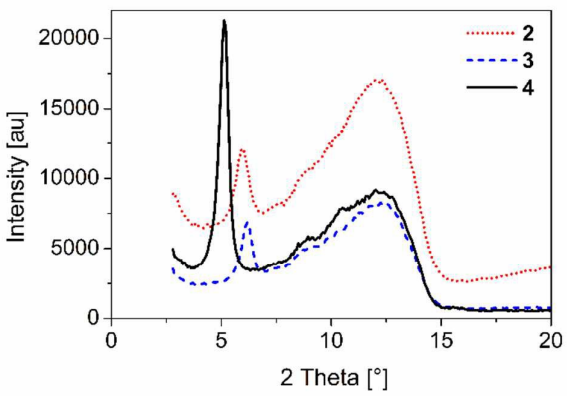

Figure 4. GIXRD plot of neat films consisting of oligomers **2**-**4** coated on glass substrate.

Table 2. Solar cell parameters for oligomers **2**-**4** using different hole transport layers (HTL). Device structure: ITO|HTL|Donor:$PC_{61}BM$ (1:2)|LiF|Al. The active D:A layer was processed from chloroform solution at 60 °C.

Donor	HTL	J_{SC} [mA cm^{-2}]	V_{OC} [V]	FF	PCE [%]
2	PEDOT:PSS	5.2	1.07	0.55	3.1
3	PEDOT:PSS	6.0	1.01	0.43	2.6
4	PEDOT:PSS	7.2	1.03	0.49	3.7
2	V_2O_5	5.1	1.10	0.62	3.5
3	V_2O_5	5.3	1.07	0.47	2.6
4	V_2O_5	7.9	1.06	0.57	4.8

Solution-processed BHJSCs with the standard device structure ITO|PEDOT:PSS|D:A blend| LiF|Al were fabricated. The obtained photovoltaic parameters are presented in Table 2 and the current density-voltage (*J*-*V*) curve and external quantum efficiency (EQE) spectra are shown in Figure S1 (see ESI†). All three oligomers **2**-**4** displayed open-circuit voltages (V_{OC}) higher than 1 V. Short-circuit current densities (J_{SC}) ranged between 5.2 - 7.2 mA cm^{-2} and fill factors (FF) between 0.43 and 0.55 were obtained leading to moderate power conversion efficiencies (PCE) of 3.1%, 2.6%, and 3.7% for **2**-, **3**- and **4**-based devices. Interestingly, upon replacement of the PEDOT:PSS hole transport layer (HTL) by a solution-processed V_2O_5 layer,[35] FFs of the devices increased to 0.47–0.62 which could be attributed to a combination of different effects. One possibility is improved hole collection at the anode associated with a better match between the work function of V_2O_5 and the HOMO energy level of the oligomer. Another possibility is that the morphology of the D:A blend is influenced by the different surface energy of V_2O_5 versus PEDOT:PSS, particularly at the interface between the hole transport and the photoactive layer. It is significant to note that the open-

circuit voltages of the photovoltaic cells increased by ~0.03 V upon replacement of PEDOT:PSS with V_2O_5, and the corresponding PCEs ranged from 2.6% to 4.8%.

Further optimization of the active layer was then carried out using V_2O_5 as HTL. The results of these experiments are shown in Table 3 and Figure 5. It was found that slight improvements in the FF were observed for **3** and **4** upon incorporation of PDMS as solvent additive.[54-56] Upon close inspection of the *J-V* characteristics, it appears that **2** and **4**-based devices display high V_{OC}s and FFs, and low saturation values. A comparatively higher FF and lowering of the saturation values are an indication of efficient charge separation and extraction.[52] The saturation value is calculated by dividing the current density measured at -1 V with that at 0 V (J_{SC}). The resulting value describes the current density dependence on the electric field strength meaning that the lower the saturation value, the lower the charge recombination process. Oligomer **3** showed the lowest PCE at 2.8% due to its low FF of 0.51. On the other hand, oligomer **4** demonstrated the highest photovoltaic parameters within the series, with a J_{SC} of 7.9 mA cm^{-2}, a V_{OC} of 1.07 V, and a FF of 0.63 giving an excellent PCE of 5.3%. Oligomer **4**-based devices were further tested using different concentration of PDMS which showed that 0.2 mg mL^{-1} of additive is optimal for obtaining high performance BHJSCs (see ESI†, Table S1). The improvement of the PCE for oligomer **4** could be ascribed to the more favorable morphology due to homogeneous distribution of the donor and acceptor component as well as controlling the ordering within the individual phases.[57,58] However, this improvement was not significant with blends of **2** and **3**; similar behaviour have also been seen in other oligomeric materials.[59] The results also suggest that the hexyl chain on the outer thiophene ring is vital in influencing the film forming properties and performance improvement of this series of oligomers.

Table 3. Solar cell parameters of oligomers **2-4** using V_2O_5 HTLs in a device structure: ITO|V_2O_5|Donor:$PC_{61}BM$ (1:2)|LiF|Al. The active layer was cast from chloroform solution using 0.2 mg mL^{-1} PDMS as an additive. The corresponding d-d distances extracted from GIXRD experiments.

Donor	J_{SC} [mA cm^{-2}]	V_{OC} [V]	FF	PCE [%]	$J_{-1\ V}/J_{SC}$	d_{100} distance [Å]
2	5.3	1.10	0.61	3.6	1.08	14.6
3	5.2	1.04	0.51	2.8	1.23	15.8
4	7.9	1.07	0.63	5.3	1.04	17.5

The external quantum efficiency (EQE) spectra of the three devices are plotted in Figure 5b. Current is being generated in the solar cells up to 750 nm with a maximum at 680 nm for **2**- and **4**-based active layers. These two donor oligomers displayed similar EQE profiles, whereas for the **3**:$PC_{61}BM$ device, the EQE profile has a quite different shape. In contrast to **2** and **4**, oligomer **3** showed two broad peaks of similar intensity at high and low energies. The high J_{SC} values obtained for **4**:$PC_{61}BM$-based devices is further reflected in the highest EQE of 62%.

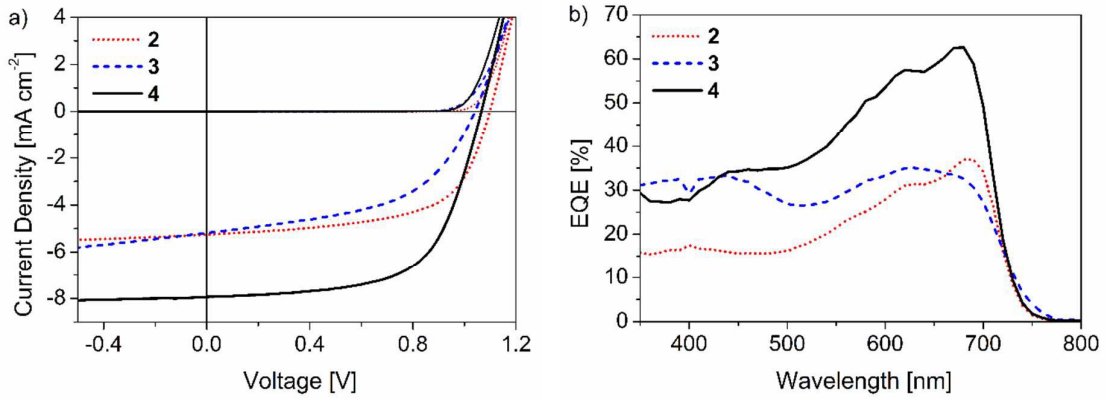

Figure 5. Comparison of *J-V* and EQE curves of the best performing solar cell devices with the optimized structure: ITO|V_2O_5|Donor:$PC_{61}BM$|LiF|Al.

In an attempt to further understand the origin of the different photovoltaic properties of oligomers **2**-**4**, UV-vis spectroscopy and grazing incident X-ray diffraction (GIXRD) measurements of the active layers were performed. In Figure 6, the absorption spectra and diffraction patterns are compared for the optimized D:A-blend films prepared using V_2O_5 as HTL and PDMS as solvent additive. The absorption profiles for the **3**:$PC_{61}BM$ blend is less defined and the maximum is blue-shifted by approximately 50 nm compared to the active layers based on oligomers **2** and **4**. On the other hand, the absorption band of **2**:$PC_{61}BM$ and **4**:$PC_{61}BM$ are quite similar (Figure 6a). The sharp onset at longer wavelengths seen in the neat films (Figure 1b), is also observed for the photoactive blends of **2** and **4** suggesting better ordering of the molecules in the blend.

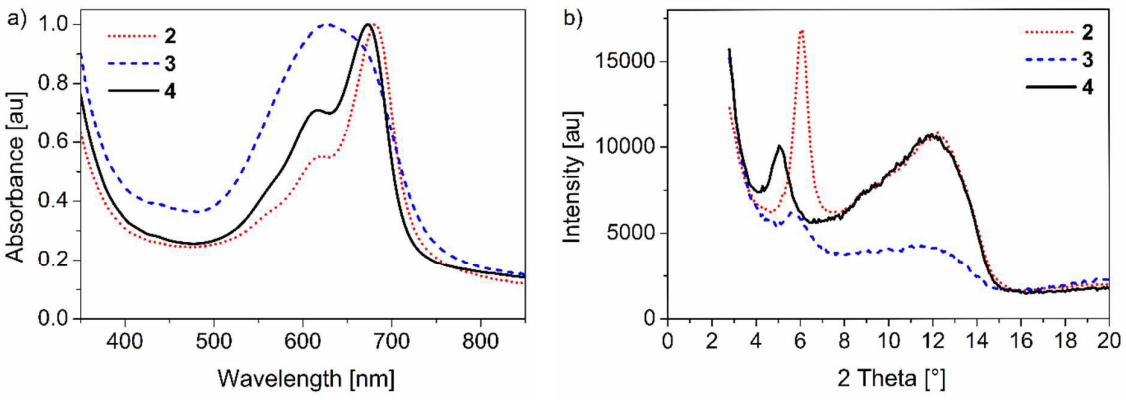

Figure 6. (a) Thin film absorption spectra and (b) 1D-GIXRD patterns of oligomer:$PC_{61}BM$ blends deposited from $CHCl_3$:PDMS on V_2O_5 coated glass substrate.

The diffraction pattern of the GIXRD measurements of the oligomer:$PC_{61}BM$ blend films processed with PDMS additive on V_2O_5-coated glass revealed insight into the organization and ordering of the oligomers (Figure 6b). The reflexes for all oligomers at low angle (2θ = 6.06° for **2**, 5.58° for **3**, 5.05° for **4**) are assigned to the packing between the adjacent oligomer backbone.[11,21] The reflection patterns measured for the neat films helped for the assignment of the reflexes observed in the blends of **2**-**4** with $PC_{61}BM$. Each oligomer displays characteristic d_{100}-distances depending on the size of their alkyl substituents and they are found to continuously increase with increasing alkyl size in the series: d_{100} = 14.6 Å for **2**, 15.8 Å for **3**, and 17.5 Å for **4** (Table 3). The intensities of the reflections at low angles and their corresponding full width at half-maximum (FWHM) revealed information about the relative crystallinity of the photoactive layers. The **2**:$PC_{61}BM$-blend had by far the highest crystallinity and was followed by **4**:$PC_{61}BM$ and **3**:$PC_{61}BM$. A similar trend is also observed for oligomer:$PC_{61}BM$-blends deposited from $CHCl_3$ on PEDOT:PSS-coated glass (see ESI†, Figure S2).

Atomic force microscopy (AFM) measurements were conducted in order to gain further insight into the surface morphology of the photoactive layers. The samples were prepared in the same way as the corresponding optimized devices, namely by spin-coating the active blends onto ITO/V_2O_5 from $CHCl_3$/PDMS solutions. The obtained AFM-images are shown in Figure 7. In addition to the more intuitively understandable topographic images, the phase images exhibited a contrast that is

produced by a complex combination of factors, such as stiffness, adhesion, or dissipation of the sample. These factors, which are usually different for the different chemical phases present for the blends of **2**-**4** with $PC_{61}BM$.

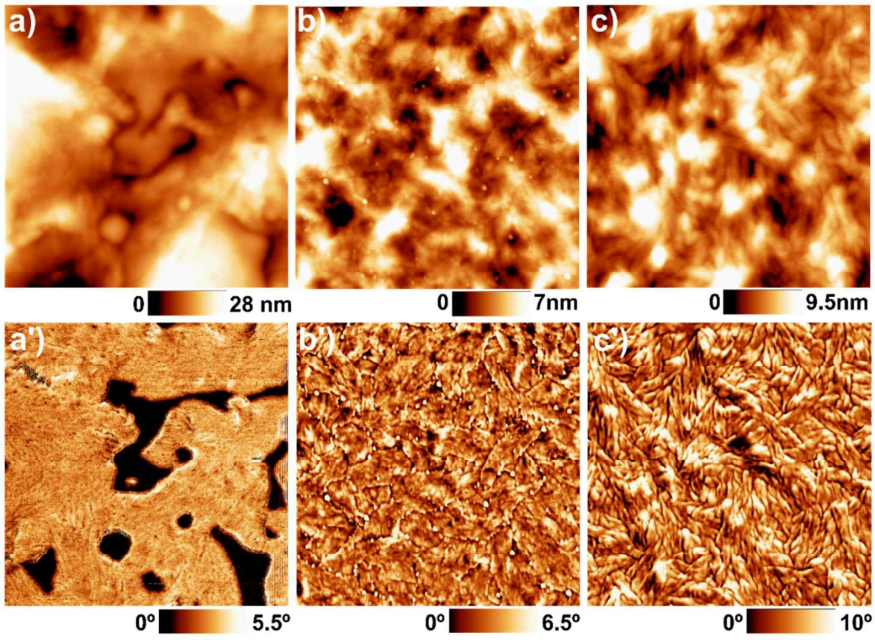

Figure 7. AFM height (a-c) and phase (a'-c') images of samples spin-coated from $CHCl_3$/PDMS solutions on ITO|V_2O_5| with (a and a') **2**:$PC_{61}BM$, (b and b') **3**:$PC_{61}BM$, and (c and c') **4**:$PC_{61}BM$. Image size: 1 x 1 µm.

Topography images (Figure 7a-c) revealed the surface landscape of the samples; topography roughness (Rq) was measured to be 7.7 ± 0.7 nm for **2**, 1.8 ± 0.1 nm for **3**, and 2.5 ± 0.1 nm for **4**. Looking at the phase images, oligomer **2** (Figure 7a') exhibited coarse phase-separation with micro-meter-ranged domains, which dramatically exceed the typical exciton diffusion length. Images of **3** and **4** (Figures 7b' and 7c', accordingly), on the contrary, showed finer structures that correlate to their more moderate roughness. With **3**, domain-size ranged from ~50 to 200 nm and domain-boundaries are decorated with small particles of bright contrast (diameter ~10-15 nm). On the other hand, for oligomer **4** elongated and distinctly defined domains with widths of ~ 10-40 nm are visible. Figure S3 (see ESI†) illustrates the three cases with a **4**:$PC_{61}BM$-blend: The active layer was spin-coated from $CHCl_3$ on either ITO/PEDOT:PSS or ITO/V_2O_5 and the optimized device from $CHCl_3$/PDMS on ITO|V_2O_5|, as analyzed in Figure 7c-c', is included for comparison. The finest

domain separation corresponds to the optimized device. We conclude from the AFM part that oligomer **2** displays coarse phase separation and high roughness, whereas **4** develops the finest domains and **3** reveals domains of intermediate size.

Now, we would like to summarize the results on active layer characterization and to correlate them to the photovoltaic properties of oligomers **2**-**4**. The absorption and GIXRD experiments revealed that **2** and **4** pack similarly and in an ordered fashion which led to high fill factors (0.61-0.62) in the solar cell devices. In the case of the **2**:$PC_{61}BM$-blend, AFM revealed a large phase separation, which correlates to the higher degree of crystallinity determined in GIXRD. The resulting high fill factors but low J_{SC} were obviously due to reduced interfacial area between the donor and acceptor phases. On the contrary, **4**:$PC_{61}BM$ layers displayed a fibrillar structure of much smaller dimension, thus yielding a finer phase separation, an increased interfacial area, and a larger charge generation in the solar cell devices. Overall, an increase of J_{SC} from 5.3 to 7.9 mA cm^{-2} is observed. The **3**:$PC_{61}BM$ blend is however not as well ordered, as evidenced by absorption and XRD spectroscopy, although the phase separation is finer than that in the **2**:$PC_{61}BM$ blend**.** In the photovoltaic devices charge transport is limited and both, FF and J_{SC} values, suffer resulting in the lowest PCE (2.8%) in the series. Correlating the above mentioned results with the chemical structures of the three oligomers, it seems reasonable to conclude that the hexyl chains attached to the outer thiophene units are necessary for good packing. It is noteworthy to mention that despite the low solubility of **2** (2 mg mL^{-1}) it still outperforms **3** (19 mg mL^{-1}) in the solar cell, stressing the importance of molecular packing over solubility, for this series of molecules.

Conclusion

In summary, we have designed and synthesized a series of dithieno[3,2-*b*:2',3'-*d*]pyrrole-based oligomers **1**-**4** for their application as donor material in bulk-heterojunction solar cells. The oligomers showed broad absorption from 500 to 700 nm with high molar absorption coefficients peaking at around 600 nm. The HOMO-LUMO energy levels estimated from electrochemical measurements

were found to be suitable for efficient charge transport to the $PC_{61}BM$ acceptor. In BHJSCs, all oligomers blend with $PC_{61}BM$ showed PCEs in the range of 2.6-3.7% when using PEDOT:PSS as hole transport layer. The performance was further improved by replacing PEDOT:PSS by a V_2O_5 layer. In order to further improve the performance, PDMS was used as solvent additive giving in particular a positive effect for oligomer **4** resulting in the highest PCE of 5.3% for this series of oligomers. The results presented here demonstrate that subtle changes in the type and size of the solubilizing alkyl substituents may have a larger impact on the photovoltaic performance. The influence of the hole transport layer and solvent additive on the morphology of the photoactive layer was investigated by absorption spectroscopy, AFM, and GIXRD. These experiments indicated that the use of V_2O_5 improves the hole transport and/or collection and the solvent additive allows for a morphological re-organization of the blend leading to higher order in the BHJ.

Experimental part

Materials and Methods: NMR spectra were recorded on a Bruker DRX 400 spectrometer (^{1}H NMR: 400 MHz, ^{13}C NMR: 100 MHz). Chemical shift values (δ) are expressed in parts per million using residual solvent protons (^{1}H NMR, δ_H = 7.26 for $CDCl_3$; ^{13}C NMR, δ_C = 77.0 for $CDCl_3$) as internal standard. The splitting patterns are designated as follows: s (singlet), d (doublet), t (triplet) and m (multiplet). Elemental analyses were performed on an Elementar Vario EL. Melting points were determined using a Mettler Toledo DSC 823. Thin layer chromatography was carried out on aluminum plates, pre-coated with silica gel, Merck Si60 F254. Preparative column chromatography was performed on glass columns packed with silica gel, Merck Silica 60, particle size 40 − 63 μm. High performance liquid chromatography was performed on a Hitachi instrument equipped with a UV-vis detector L-7420, columns (Nucleosil 100-5 NO_2 with a pore size of 100 Å) from Machery-Nagel using a dichloromethane/n-hexane mixture (40:60) as eluent. EI mass spectra were recorded on a Varian Saturn 2000 GC-MS, MALDI-MS experiments were performed using a MS Bruker Reflex 2 (Bruker Daltonik GmbH, Bremen, Germany) using trans-2-[3-(4-tert-butylphenyl)-2-methyl-

2-pro-penylidene] malononitrile (DCTB) as matrix. UV/Vis absorption spectra were recorded in 1 cm cuvettes with Merck Uvasol grade solvents on a Perkin Elmer Lambda 19 spectrometer. Cyclic voltammetry experiments were performed with a computer-controlled Autolab PGSTAT30 potentiostat in a three-electrode single-compartment cell with a platinum working electrode, a platinum wire counter electrode, and a Ag/AgCl reference electrode. All potentials were internally referenced to the ferrocene/ferricenium couple. Tetrahydrofuran and N,N-dimethylformamide (Merck) were dried using a MB SPS-800 solvent purifying system (MBraun). All synthetic steps were carried out under argon atmosphere. Tetrakis(triphenylphosphine)palladium(0) was prepared according to a literature known procedure. XRD measurements were carried out using a Bruker D8 diffractometer with a fixed incoming angle of 0.2°. Surface images of photoactive layers were recorded with the help of an atomic force microscope (MultiMode V AFM, Bruker). The microscope was operated in air at room temperature in the tapping mode using commercial silicon tips with a resonance frequency of 200–400 kHz and spring constants of ≈50 N m $^{-1}$. The images were analyzed with the help of the WSxM software.[60]

Device fabrication: Photovoltaic devices were made by spin-coating PEDOT:PSS (Clevios P, VP Al4083) onto pre-cleaned, patterned indium tin oxide (ITO) substrates (15 Ω per square) (Kintec). The photoactive layer (~80 nm) was deposited by spin-coating from of a mixed solution of donor with $PC_{61}BM$ (total concentration of 15 mg/mL in $CHCl_3$) at 60°C. For the devices made with poly(dimethylsiloxane) (PDMS) as additive, a stock solution of 0.2 mg/mL PDMS in $CHCl_3$ was used. $PC_{61}BM$ was purchased from Solenne BV, Netherlands. The counter electrode of LiF (1 nm) and aluminum (100 nm) was deposited by vacuum evaporation at 2 x 10^{-6} Torr. Sol-gel method involves making a solution of vanadium(V) oxytriisopropoxide [$VO(OC_3H_7)_3$] in isopropyl alcohol. Hydrolysis begins upon spin-coating of $VO(OC_3H_7)_3$ at 5750 rpm and is complete after exposure to ambient conditions with a relative humidity of 60% for 60 minutes without any heating to form thin layer of V_2O_5. The work function of V_2O_5 was reported to be 5.6 eV.[35] The active areas of the cells were 0.1 cm^2. Film thicknesses were measured using a Dektak profilometer. J-V characteristics

were measured under AM 1.5G conditions at 100 mW cm^{-2} with a AAA solar simulator from Oriel Instruments using a Keithley 2400 source meter. Spectral response was measured under monochromatic light from a 300 W Xenon lamp in combination with a monochromator (Oriel, Cornerstone 260) modulated with a mechanical chopper. The response was recorded as the voltage over a 220 Ω resistance, using a lock-in amplifier (Merlin 70104). A calibrated Si-cell was used as reference. The devices were kept behind a quartz window in a nitrogen filled container.

Synthesis: **2,2'-(5,5'-[N-{2-Ethylhexyl}dithieno[3,2-b:2',3'-d]pyrrole-2,6-diyl]-bis(methane-1-yl-1-ylidine)dimalononitrile (1)**. A mixture of 4-(2-ethylhexyl)-2,6-bis(trimethylstannyl)dithieno[3,2-*b*:2',3'-*d*]pyrrol **5a** (0.218 g, 0.353 mmol), 2-bromo-5-(2,2-dicyanovinyl)thiophene **6** (0.177 g, 0.742 mmol) and $Pd(PPh_3)_4$ (0.02 g, 17.7 µmol) was combined in degassed DMF (100 mL) and stirred at 80 °C for 20 hours. After cooling, the resulting precipitate was filtered off and washed several times with methanol. After drying, Oligomer **1** (0.190 g, 0.313 mmol, 83%) was obtained as a dark green solid. M.p. 301 °C (DSC). ^{1}H NMR (tetrachloroethane-d_2, 100 °C, δ ppm) 7.71 (s, 2H, C=CH), 7.61 (d, 2H, *J* = 4.2 Hz, Th*H*), 7.30 (d, 2H, *J* = 4.1 Hz, Th*H*), 7.28 (s, 2H, Th*H*); 4.11-4.05 (m, 2H, N-CH_2), 1.98 (m, 1H, -C*H*-), 1.35 (m, 8H, -CH_2-), 0.92 (t, 3H, *J* = 7.4 Hz, -CH_3), 0.87 (t, 3H, *J* = 7.0 Hz, -CH_3). HRMS (MALDI-TOF) *m/z*: calcd. for $C_{32}H_{25}N_5S_4$ 607.09928; found 607.09866 [M^+] (*δm/m* = 1.0 ppm).

2,2'-(5,5'-[N-{2-Ethylhexyl}dithieno[3,2-b:2',3'-d]pyrrole-2,6-diyl]-bis[3-hexylthien-5,2-diyl])-bis(methane-1-yl-1-ylidine)dimalononitrile (2). 4-(2-Ethylhexyl)-2,6-bis(trimethylstannyl)dithieno[3,2-*b*:2',3'-*d*]pyrrol **5a** (58.9 mg, 95.4 µmol), 2-iodo-4-hexyl-5-(2,2-dicyanovinyl)thiophene **7** (89.8 mg, 243 µmol) and $Pd(PPh_3)_4$ (6.8 mg, 5.91 µmol) were added in a Schlenk-tube and evacuated for about 10 minutes. After addition of DMF (5 mL), the reaction mixture was carefully degassed and heated to 60 °C for 3.5 h. Then the reaction mixture was poured into saturated aqueous NH_4Cl solution. The organic compounds were extracted with DCM. The combined organic phases were dried with Na_2SO_4 and the solvents were removed by rotary evaporation. The crude product was purified via digesting with ethyl acetate and subsequent column chromatography using silica

(DCM) to obtain oligomer **2** (60.0 mg, 77.3 μmol, 81%) as a dark solid. M.p.: 309 °C. ^{1}H NMR (400 MHz, $CDCl_3$, δ) 7.80 (s, 2H, C=C*H*), 7.28 (s, 2H, Th*H*), 7.13 (s, 2H, Th*H*), 4.13-4.03 (m, 2H, N-CH_2), 2.74 (t, *J* = 7.8 Hz, 4H, α-CH_2), 2.04-1.95 (m, 1H, -C*H*-), 1.69-1.61 (m, 4H, β-CH_2), 1.44-1.27 (m, 20H, -CH_2-), 0.94-0.89 (m, 12H, -CH_3). ^{13}C NMR (100 MHz, $CDCl_3$, δ ppm) 157.06, 148.74, 147.22, 146.91, 134.78, 128.74, 125.46, 117.51, 115.06, 114.03, 110.53, 73.99, 52.13, 40.35, 31.54, 31.21, 30.75, 29.32, 29.06, 28.59, 24.26, 23.02, 22.51, 13.92, 13.89, 10.74. HRMS (MALDI-TOF) *m/z*: calcd for $C_{44}H_{49}N_5S_4$: 775.28708; found $[M]^+$: 775.28628 (*δm/m* = 1.0 ppm).

2,2'-(5,5'-[N-{1-Octylnonyl}dithieno[3,2-b:2',3'-d]pyrrole-2,6-diyl]-bis(methane-1-yl-1-ylidine)dimalononitrile (3). In a Schlenk tube, 2,6-bis(trimethylstannyl)-4-(1-octylnonyl)dithieno[3,2-*b*:2′,3′-*d*]pyrrole **5b** (0.2 g, 0.27 mmol), 2-[(5-bromothien-2-yl)methylene]malononitrile **6** (0.15 g, 0.64 mmol) and $Pd(PPh_3)_4$ (0.015 g, 13.4 μmol) were dissolved in dry DMF (5 mL) and the solution was purged with argon for 10–15 minutes. The solution was then stirred at 60 °C for 19 h. After completion the reaction mixture was poured into saturated aqueous NH_4Cl solution. The organic phase was extracted with DCM. The combined organic phases were dried over Na_2SO_4 and the solvents were removed by rotary evaporation. The crude product was purified by column chromategraphy on silica gel (eluent DCM) to yield pure oligomer **3** as a dark solid (144 mg, 0.196 mmol, 73%). M.p.: 233 °C. ^{1}H NMR (400 MHz, $CDCl_3$, δ) 7.76 (s, 2H, C=C*H*), 7.60 (d, 2H, *J* = 4.2 Hz, Th*H*), 7.35 (s, 2H, Th*H*), 7.30 (d, 2H, *J* = 4.2 Hz, Th*H*), 4.30-4.17 (m, 1H, N-C*H*), 2.10-1.85 (m, 4H, -CH_2-), 1.36-1.0 (m, 24H, -CH_2-), 0.81 (t, *J* = 6.9 Hz, 6H, -CH_3). ^{13}C NMR (100 MHz, $CDCl_3$, δ ppm) 157.38, 148.93, 147.09, 134.53, 128.50, 125.43, 115.29, 114.26, 111.23, 73.13, 34.97, 31.78, 29.33, 29.09, 26.73, 22.65, 22.59, 14.10. HRMS (MALDI-TOF) *m/z*: calcd for $C_{41}H_{43}N_5S_4$ 733.24013; found $[M]^+$: 733.23935 (*δm/m* = 2.2 ppm).

2,2'-(5,5'-[N-{1-Octylnonyl}dithieno[3,2-b:2',3'-d]pyrrole-2,6-diyl]-bis[3-hexylthien-5,2-diyl])-bis(methane-1-yl-1-ylidine)dimalononitrile (4). In a Schlenk tube, 2,6-bis(trimethylstannyl)-4-(1-octylnonyl)dithieno[3,2-*b*:2′,3′-*d*]pyrrole **5b** (0.2 g, 0.27 mmol), 2-((3-hexyl-5-iodothien-2-yl)methylene)malononitrile **7** (0.24 g, 0.64 mmol) and $Pd(PPh_3)_4$ (0.015 g, 13.4 μmol) were dissolved in

dry DMF (5 mL) and the solution was carefully degassed with argon and stirred at 60 °C for 18 h. Subsequently, the reaction mixture was cooled down to room temperature and poured into saturated ammonium chloride solution. The organic phase was extracted with dichloromethane followed by drying over Na_2SO_4 and removal of the solvents. After column chromatography using SiO_2 (DCM) the pure product **4** (0.186 g, 0.20 mmol) was isolated as a dark solid in 77% yield. M.p.: 280 °C. ^{1}H NMR (400 MHz, $CDCl_3$, δ) 7.80 (s, 2H, C=C*H*), 7.34 (s, 2H, Th*H*), 7.14 (s, 2H, Th*H*), 4.27-4.17 (m, 1H, N-C*H*), 2.74 (t, *J* = 7.8 Hz, 4H, α-CH_2), 2.10-1.85 (m, 4H, -CH_2-), 1.70-1.60 (m, 4H, β-CH_2), 1.45-1.0 (m, 36H, -CH_2-), 0.91 (t, *J* = 6.9 Hz, 6H, -CH_3), 0.81 (t, *J* = 6.9 Hz, 6H, -CH_3). ^{13}C NMR (100 MHz, $CDCl_3$, δ ppm) 157.37, 148.95, 147.10, 134.51, 128.49, 125.42, 115.29, 114.24, 111.22, 73.14, 60.94, 34.99, 31.79, 31.56, 31.33, 29.35, 29.30, 29.25, 29.15, 29.10, 26.72, 22.64, 22.58, 14.10. HRMS (MALDI-TOF) *m/z*: calcd for $C_{53}H_{67}N_5S_4$: 901.42793; found $[M]^+$: 901.42703 ($\delta m/m$ = 0.99 ppm).

Acknowledgements

We thank the Baden-Württemberg-Stiftung for funding this work as part of the research program "Organic Photovoltaics & Dye Solar Cells". PK would like to acknowledge the Alexander von Humboldt Foundation for financial support. MU thank the Spanish MINECO (MAT2010-21156-C03-03) and the University of the Basque Country (EHUA12/05) for their support of this work. We are grateful to Kirill Zilberberg and Prof. Thomas Riedl from University of Wuppertal for their support in processing the metal oxide layers. We would like to thank Samuel Blessing (Institute of Inorganic Chemistry I, University of Ulm) for carrying out the XRD measurements.

References

1. A. K. K. Kyaw, D. H. Wang, D. Wynands, J. Zhang, T.-Q. Nguyen, G. C. Bazan and A. J. Heeger, *Nano Lett.*, 2013, **13**, 3796-3801.
2. B. Kan, Q. Zhang, M. Li, X. Wan, W. Ni, G. Long, Y. Wang, X. Yang, H. Feng and Y. Chen, *J. Am. Chem. Soc.*, 2014, **136**, 15529–15532.
3. K. Sun, Z. Xiao, S. Lu, W. Zajaczkowski, W. Pisula, E. Hanssen, J. M. White, R. M. Williamson, J. Subbiah, J. Ouyang, A. B. Holmes, W. W. H. Wong and D. J. Jones, *Nat. Commun.*, 2015, **6**, 6013.

4. Q. Zhang, B. Kan, F. Liu, G. Long, X. Wan, X. Chen, Y. Zuo, W. Ni, H. Zhang, M. Li, Z. Hu, F. Huang, Y. Cao, Z. Liang, M. Zhang, T. P. Russell and Y. Chen, *Nat. Photon.*, 2015, **9**, 35–41.
5. B. Kan, M. Li, Q. Zhang, F. Liu, X. Wan, Y. Wang, W. Ni, G. Long, X. Yang, H. Feng, Y. Zuo, M. Zhang, F. Huang, Y. Cao, T. P. Russell and Y. Chen, *J. Am. Chem. Soc.*, 2015, **137**, 3886–3893.
6. Y. Liu, C.-C. Chen, Z. Hong, J. Gao, Y. M. Yang, H. Zhou, L. Dou, G. Li and Y. Yang, *Sci. Rep.*, 2013, **3**, 3356, doi:3310.1038/srep03356.
7. Y.-H. Chen, L.-Y. Lin, C.-W. Lu, Z.-Y. Huang, H.-W. Lin, F. Lin, P.-H. Wang, Y.-H. Liu, K.-T. Wong, J. Wen, D. J. Miller and S. B. Darling, *J. Am. Chem. Soc.*, 2012, **134**, 13616–13623.
8. H.-W. Lin, J.-H. Chang, W.-C. Huang, Y.-T. Lin, L.-Y. Lin, F. Lin, K.-T. Wong, H.-F. Wang, R.-M. Ho and H.-F. Meng, *J. Mater. Chem. A*, 2014, **2**, 3709-3714.
9. T. S. van der Poll, J. A. Love, T.-Q. Nguyen and G. C. Bazan, *Adv. Mater.*, 2012, **24**, 3646–3649.
10. X. Liu, Y. Sun, B. B. Y. Hsu, A. Lorbach, L. Qi, A. J. Heeger and G. C. Bazan, *J. Am. Chem. Soc.*, 2014, **136**, 5697–5708.
11. C. D. Wessendorf, G. L. Schulz, A. Mishra, P. Kar, I. Ata, M. Weidelener, M. Urdanpilleta, J. Hanisch, E. Mena-Osteritz, M. Lindén, E. Ahlswede and P. Bäuerle, *Adv. Energy Mater.*, 2014, **4**, 1400266.
12. A. Mishra and P. Bäuerle, *Angew. Chem. Int. Ed.*, 2012, **51**, 2020–2067.
13. Y. Lin, Y. Li and X. Zhan, *Chem. Soc. Rev.*, 2012, **41**, 4245-4272.
14. J. E. Coughlin, Z. B. Henson, G. C. Welch and G. C. Bazan, *Acc. Chem. Res.*, 2014, **47**, 257–270.
15. Y. Chen, X. Wan and G. Long, *Acc. Chem. Res.*, 2013, **46**, 2645-2655.
16. V. Malytskyi, J.-J. Simon, L. Patrone and J.-M. Raimundo, *RSC Adv.*, 2015, **5**, 354-397.
17. Y. Sun, G. C. Welch, W. L. Leong, C. J. Takacs, G. C. Bazan and A. J. Heeger, *Nat. Mater.*, 2012, **11**, 44–48.
18. Y. Liu, X. Wan, F. Wang, J. Zhou, G. Long, J. Tian and Y. Chen, *Adv. Mater.*, 2011, **23**, 5387–5391.
19. J. Zhou, X. Wan, Y. Liu, G. Long, F. Wang, Z. Li, Y. Zuo, C. Li and Y. Chen, *Chem. Mater.*, 2011, **23**, 4666–4668.
20. Z. Li, G. He, X. Wan, Y. Liu, J. Zhou, G. Long, Y. Zuo, M. Zhang and Y. Chen, *Adv. Energy Mater.*, 2012, **2**, 74–77.
21. M. Weidelener, C. D. Wessendorf, J. Hanisch, E. Ahlswede, G. Götz, M. Lindén, G. Schulz, E. Mena-Osteritz, A. Mishra and P. Bäuerle, *Chem. Commun.*, 2013, **49**, 10865-10867.
22. G. C. Welch, L. A. Perez, C. V. Hoven, Y. Zhang, X.-D. Dang, A. Sharenko, M. F. Toney, E. J. Kramer, T.-Q. Nguyen and G. C. Bazan, *J. Mater. Chem.*, 2011, **21**, 12700-12709.
23. Z. B. Henson, G. C. Welch, T. van der Poll and G. C. Bazan, *J. Am. Chem. Soc.*, 2012, **134**, 3766–3779.
24. G. Schulz, M. Lobert, I. Ata, M. Urdanpilleta, M. Linden, A. Mishra and P. Bäuerle, *J. Mater. Chem. A*, 2015, **3**, 13738-13748.
25. S. C. Rasmussen and S. J. Evenson, *Prog. Polym. Sci.*, 2013, **38**, 1773–1804.
26. R. Grisorio, G. Allegretta, G. P. Suranna, P. Mastrorilli, A. Loiudice, A. Rizzo, M. Mazzeo and G. Gigli, *J. Mater. Chem.*, 2012, **22**, 19752-19760.
27. A. Yassin, P. Leriche, M. Allain and J. Roncali, *New J. Chem.*, 2013, **37**, 502-507.
28. B. H. Wunsch, M. Rumi, N. R. Tummala, C. Risko, D.-Y. Kang, K. X. Steirer, J. Gantz, M. Said, N. R. Armstrong, J.-L. Bredas, D. Bucknall and S. R. Marder, *J. Mater. Chem. C*, 2013, **1**, 5250-5260.
29. L. G. Mercier, A. Mishra, Y. Ishigaki, F. Henne, G. Schulz and P. Bäuerle, *Org. Lett.*, 2014, **16**, 2642–2645.
30. J. Meyer, S. Hamwi, M. Kröger, W. Kowalsky, T. Riedl and A. Kahn, *Adv. Mater.*, 2012, **24**, 5408–5427.
31. S. Chen, J. R. Manders, S.-W. Tsang and F. So, *J. Mater. Chem.*, 2012, **22**, 24202-24212.
32. F. Xie, W. C. H. Choy, C. Wang, X. Li, S. Zhang and J. Hou, *Adv. Mater.*, 2013, **25**, 2193–2199.
33. H.-Q. Wang, N. Li, N. S. Guldal and C. J. Brabec, *Org. Electron.*, 2012, **13**, 3014-3021.
34. K. Zilberberg, S. Trost, J. Meyer, A. Kahn, A. Behrendt, D. Lützenkirchen-Hecht, R. Frahm and T. Riedl, *Adv. Funct. Mater.*, 2011, **21**, 4776–4783.
35. K. Zilberberg, S. Trost, H. Schmidt and T. Riedl, *Adv. Energy Mater.*, 2011, **1**, 377-381.
36. S. Murase and Y. Yang, *Adv. Mater.*, 2012, **24**, 2459–2462.
37. Z. a. Tan, D. Qian, W. Zhang, L. Li, Y. Ding, Q. Xu, F. Wang and Y. Li, *J. Mater. Chem. A*, 2013, **1**, 657-664.
38. T. Stubhan, N. Li, N. A. Luechinger, S. C. Halim, G. J. Matt and C. J. Brabec, *Adv. Energy Mater.*, 2012, **2**, 1433–1438.

39. Z. a. Tan, L. Li, C. Cui, Y. Ding, Q. Xu, S. Li, D. Qian and Y. Li, *J. Phys. Chem. C*, 2012, **116**, 18626-18632.
40. M. D. Irwin, D. B. Buchholz, A. W. Hains, R. P. H. Chang and T. J. Marks, *Proc. Nat. Acad. Sci.*, 2008, **105**, 2783-2787.
41. J. R. Manders, S.-W. Tsang, M. J. Hartel, T.-H. Lai, S. Chen, C. M. Amb, J. R. Reynolds and F. So, *Adv. Funct. Mater.*, 2013, **23**, 2993–3001.
42. A. Garcia, G. C. Welch, E. L. Ratcliff, D. S. Ginley, G. C. Bazan and D. C. Olson, *Adv. Mater.*, 2012, **24**, 5368–5373.
43. C. E. Song, K. Y. Ryu, S.-J. Hong, C. Bathula, S. K. Lee, W. S. Shin, J.-C. Lee, S. K. Choi, J. H. Kim and S.-J. Moon, *ChemSusChem*, 2013, **6**, 1445–1454.
44. S. Chen, C. E. Small, C. M. Amb, J. Subbiah, T.-h. Lai, S.-W. Tsang, J. R. Manders, J. R. Reynolds and F. So, *Adv. Energy Mater.*, 2012, **2**, 1333-1337.
45. J. Jo, J.-R. Pouliot, D. Wynands, S. D. Collins, J. Y. Kim, T. L. Nguyen, H. Y. Woo, Y. Sun, M. Leclerc and A. J. Heeger, *Adv. Mater.*, 2013, **25**, 4783–4788.
46. C. E. Small, S. Chen, J. Subbiah, C. M. Amb, S.-W. Tsang, T.-H. Lai, J. R. Reynolds and F. So, *Nat. Photon.*, 2012, **6**, 115-120.
47. H. Choi, J. S. Park, E. Jeong, G.-H. Kim, B. R. Lee, S. O. Kim, M. H. Song, H. Y. Woo and J. Y. Kim, *Adv. Mater.*, 2011, **23**, 2759-2763.
48. M.-H. Park, J.-H. Li, A. Kumar, G. Li and Y. Yang, *Adv. Funct. Mater.*, 2009, **19**, 1241-1246.
49. C.-C. Chueh, C.-Z. Li and A. K. Y. Jen, *Energy Environ. Sci.*, 2015, **8**, 1160-1189.
50. K. Zilberberg, J. Meyer and T. Riedl, *J. Mater. Chem. C*, 2013, **1**, 4796-4815.
51. R. Fitzner, E. Mena-Osteritz, A. Mishra, G. Schulz, E. Reinold, M. Weil, C. Körner, H. Ziehlke, C. Elschner, K. Leo, M. Riede, M. Pfeiffer, C. Uhrich and P. Bäuerle, *J. Am. Chem. Soc.*, 2012, **134**, 11064–11067.
52. R. Fitzner, E. Reinold, A. Mishra, E. Mena-Osteritz, H. Ziehlke, C. Körner, K. Leo, M. Riede, M. Weil, O. Tsaryova, A. Weiß, C. Uhrich, M. Pfeiffer and P. Bäuerle, *Adv. Funct. Mater.*, 2011, **21**, 897-910.
53. J. C. Hummelen, B. W. Knight, F. LePeq, F. Wudl, J. Yao and C. L. Wilkins, *J. Org. Chem.*, 1995, **60**, 532-538.
54. K. R. Graham, J. Mei, R. Stalder, J. W. Shim, H. Cheun, F. Steffy, F. So, B. Kippelen and J. R. Reynolds, *ACS Appl. Mater. Interfaces*, 2011, **3**, 1210-1215.
55. K. R. Graham, P. M. Wieruszewski, R. Stalder, M. J. Hartel, J. Mei, F. So and J. R. Reynolds, *Adv. Funct. Mater.*, 2012, **22**, 4801–4813.
56. F. Hermerschmidt, A. S. Kalogirou, J. Min, G. A. Zissimou, S. M. Tuladhar, T. Ameri, H. Faber, G. Itskos, S. A. Choulis, T. D. Anthopoulos, D. D. C. Bradley, J. Nelson, C. J. Brabec and P. A. Koutentis, *J. Mater. Chem. C*, 2015, **3**, 2358-2365.
57. M.-S. Su, C.-Y. Kuo, M.-C. Yuan, U. S. Jeng, C.-J. Su and K.-H. Wei, *Adv. Mater.*, 2011, **23**, 3315-3319.
58. J. T. Rogers, K. Schmidt, M. F. Toney, E. J. Kramer and G. C. Bazan, *Adv. Mater.*, 2011, **23**, 2284-2288.
59. J. Zhou, X. Wan, Y. Liu, Y. Zuo, Z. Li, G. He, G. Long, W. Ni, C. Li, X.-C. Su and Y. Chen, *J. Am. Chem. Soc.*, 2012, **134**, 16345–16351.
60. I. Horcas, R. Fernández, J. M. Gómez-Rodríguez, J. Colchero, J. Gómez-Herrero and A. M. Baro, *Rev. Sci. Instrum.*, 2007, **78**, 013705.

Table of Content

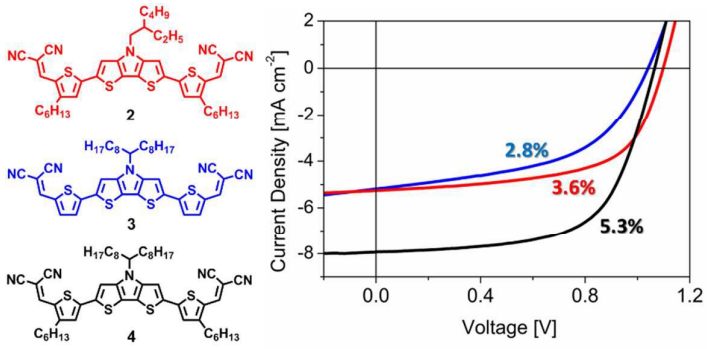

Dithienopyrrole-based small molecular materials were developed achieving PCEs up to 5.3% in bulk-heterojunction organic solar cells by the tuning of the alkyl substitution pattern and use of solvent additive.